Cytokinetic furrowing and abscission dynamics during brain development revealed by live imaging

Katrina C. McNeely[1,2], Jessica Neville Little[1,3,4], and Noelle D. Dwyer[1*]

[1]Department of Cell Biology, [2]Neuroscience Graduate Program, [3]Cell and Developmental Biology Graduate Program and [4]Medical Scientist Training Program, University of Virginia School of Medicine, Charlottesville, VA 22908, USA *To whom correspondence should be addressed at: University of Virginia Department of Cell Biology, PO Box 800732, Charlottesville, VA 22908, USA. Tel: 434-982-0692; Fax: 434-297-5546; Email: ndwyer@virginia.edu

Running Title

Cytokinetic furrowing and abscission in NESCs

Keywords

Cytokinesis, Midbody, Microcephaly, Mouse, Stem Cell, Cerebral Cortex

Summary

McNeely et al. quantitatively analyze polarized cytokinetic furrow ingression and abscission in mouse neuroepithelium by live imaging. The findings show important differences from HeLa cells, and suggest abscission timing and midbody release may be developmentally regulated, to influence daughter cell fate during brain growth.

Abstract

While mechanisms of cytokinesis have been identified in single cell models, the spatial and temporal regulation in developing tissues is less understood. Here we compare cytokinetic furrowing and abscission in mouse neuroepithelial stem cells (NESCs) at different developmental stages and in a cytokinesis mutant, including imaging abscission dynamics in a polarized epithelium for the first time. We find that asymmetric furrows of NESCs ingress at a constant but slow rate, and form the midbody at the apical membrane. Usually, bilateral abscission on each midbody flank releases the midbody remnant extracellularly. Interestingly, midbody remnants are more associated with early proliferative divisions. Unexpectedly, in the microcephalic *Kif20b* mutant, abscission is accelerated and occurs when the midbody is wider. The daughter cells of mutant NESCs show increased cell cycle exit that is p53-independent. We suggest that abscission mechanisms are developmentally regulated. These results provide significant insight into adaptations of a fundamental cell biological process required for proper brain growth.

Introduction

Regulation of cytokinesis is essential for the formation of every tissue in the body. However, the roles of cytokinesis in building multicellular tissues have only begun to be addressed. In particular, the temporal and spatial regulation of cytokinetic abscission during development remains mysterious.

The basic mechanisms of cytokinetic furrowing and abscission have been established from studies in single cell models (Green et al., 2012; Nahse et al., 2017). After chromosome segregation, the central spindle induces cleavage furrow ingression at the midzone. Upon furrow completion, the central spindle microtubules are compacted into a structure called the midbody within the intercellular bridge. The midbody contains over 150 proteins that assemble into domains including a central bulge (Flemming body) and lateral flanks (Mierzwa and Gerlich, 2014; Skop et al., 2004). This organelle mediates abscission, the process of severing the intercellular bridge. Abscission involves both microtubule disassembly and plasma membrane scission at constriction sites on midbody flanks (Connell et al., 2009; Guizetti et al., 2011). Interestingly, abscission has been variously reported to occur on only one or on both midbody flanks in different cell types. Abscission on one flank results in midbody inheritance by the contralateral daughter, whereas bilateral abscission on both flanks releases the central bulge extracellularly as a midbody remnant (MBR). Accumulating evidence from worms, flies, and cell lines suggests that temporal and spatial regulation of abscission, as well as MBRs, can influence daughter cell polarity and fate (Dionne et al., 2015; Ettinger et al., 2011; Kuo et al., 2011; Lenhart and DiNardo, 2015; Pollarolo et al., 2011; Salzmann et al., 2014; Singh and Pohl, 2014). More study is needed to

understand how the core mechanisms of cytokinesis identified in simple models evolved and adapted in mammalian tissues, such as the growing brain.

Neuroepithelial stem cells (NESCs) of the cerebral cortex appear to be especially vulnerable to perturbations in cytokinesis, perhaps because of their need to maintain polarity and produce the neurons and glia of the brain in a short developmental window. In fact, mouse and human mutations in genes encoding midbody proteins cause devastating lethal microcephaly (Bondeson et al., 2017; Di Cunto et al., 2000; Frosk et al., 2017; Janisch et al., 2013; Li et al., 2016). NESCs are highly polarized cells, with apical endfeet attached by junctions that line the lateral ventricle, and long basal processes that contact the pia. Importantly, their nuclei move to the apical membrane for mitosis and cytokinesis. Cleavage furrows ingress asymmetrically from basal to apical, and form midbodies at the apical membrane. At first, NESCs perform symmetric proliferative divisions to produce two NESC daughters and expand the epithelial area. As development progresses, NESCs increase neurogenic divisions, producing neuronal daughters that exit the cell cycle, detach from the apical membrane, and migrate away from the ventricle (Bizzotto and Francis, 2015; Dwyer et al., 2016). The mechanisms that control the change from proliferative to neurogenic divisions remain poorly understood. Candidate fate determinants include apical cell components that are segregated during furrowing and abscission, including apical junctions, Notch/Numb, centrosomes, and the midbody itself (Dubreuil et al., 2007; Higashi et al., 2016; Kim et al., 2010; Paridaen and Huttner, 2014).

Previously, we showed that mutation of the Kinesin-6 *Kif20b* in mice causes defects in cortical NESC midbody structure, an increase in NESC apoptosis, and

microcephaly (Dwyer et al., 2011; Janisch et al., 2013). The midbody structural defects are cell autonomous, and not due to apoptosis (Little and Dwyer, 2019). Kif20b localizes to the central spindle, then midbody flanks and constriction sites (Abaza et al., 2003; Janisch et al., 2018). We found that in HeLa cells, Kif20b depletion disrupted furrowing speed, midbody maturation and abscission timing, but not completion (Janisch et al., 2018). It is remarkable that subtle defects in cytokinesis may cause apoptosis in NESCs and severely disrupt brain growth; this underscores the need for more studies of cytokinesis perturbations in stem cells.

Here we perform for the first time, quantitative analysis of cytokinetic furrow ingression and abscission in NESCs through live imaging of cortical neuroepithelium. We analyze temporal and spatial regulation of abscission at different developmental stages, and in the microcephalic *Kif20b* mutant. We note important similarities and differences between NESC and HeLa cell findings. Our data suggest that abscission timing and midbody disposal are regulated differently in proliferative and neurogenic NESC divisions. Kif20b loss does not cause abscission failure or delay, but surprisingly causes accelerated abscission and increased cell cycle exit. NESC abscission is usually bilateral, releasing the midbody remnant onto the apical membrane, consistent with the idea that the MBR has cell to cell signaling potential.

Results and Discussion

Asymmetric furrow ingression in cortical NESCs is smooth and relatively slower than HeLa cells

It has been shown in fixed brain studies that cortical NESCs furrow asymmetrically, usually at an angle perpendicular to the apical membrane (schematic 1A, A'). However, furrow ingression kinetics have never been analyzed in these cells, or in mutants that disrupt cytokinesis. Our previous *in vivo* data from fixed brains suggested that loss of Kif20b in the cortex did not disrupt cleavage furrowing of NESCs: furrow angles were normal, and binucleate cells were not detectable in mutant brains (Janisch et al., 2013). Later we showed in live HeLa cells that acute depletion of Kif20b did not prevent furrow ingression or completion, but slightly reduced the rate of ingression (Janisch et al., 2018). We wanted to test how accurately HeLa cell data would model cleavage furrowing in an epithelium with complex 3-dimensional architecture.

To analyze NESC furrow ingression with live time-lapse imaging, we adapted our previously established fixed cortical slab explant method (Janisch and Dwyer, 2016). Dissecting cortical slabs from membrane-GFP transgenic mice, and labeling polymerized microtubules with SiR-Tubulin enabled us to find NESCs in mitosis at the apical membrane and follow them through cytokinesis. Despite the photo-sensitivity of NESCs, we were able to collect images every 3 minutes.

These analyses reveal important differences in furrow ingression between NESCs and HeLa cells. After the NESC apical process rounds up in mitosis, in anaphase it elongates parallel to the apical membrane (along the spindle axis). Then the furrow initiates on the basal side, and ingresses asymmetrically towards the apical membrane as a contractile arch, rather than a concentric ring (Fig. 1B, C). In both control and *Kif20b* mutant cells, ingression proceeds at a constant rate without pauses

or regressions, over ~15 minutes until completion (Fig. 1D). Interestingly, the rate of furrow ingression is almost 10-fold slower than we previously observed in HeLa cells (0.4 μm/min vs 3.8 μm/min (Janisch et al., 2018). Furthermore, the furrow rate of *Kif20b* mutant NESCs matches that of controls, and the pole-to-pole elongation rate also matches (Fig. 1D, E). By contrast, in HeLa cells, both furrowing and elongation rates were slowed by Kif20b depletion. The *Kif20b* mutant NESCs had a slightly larger starting width, requiring ~3 minutes more to complete the furrow (Fig. 1D, F). Together, these data show that NESCs have asymmetric furrow ingression in the basolateral membrane that proceeds at a relatively slow but constant rate, and the total time to furrow completion is proportional to the starting diameter. Further, the absence of furrow regression in *Kif20b* mutant NESCs explains why we have not found binucleate brain cells in the mutants. Finally, the differences between HeLa cell and NESC furrowing, and the discordant effects on ingression rate between Kif20b depletion in HeLa and Kif20b loss in NESCs, highlight the need for more studies of cytokinesis in polarized epithelia.

Abscission duration is highly variable in NESCs but accelerated in Kif20b mutants

Mechanisms and kinetics of cytokinetic abscission have been predominantly studied in HeLa cells, but these are cancer cells that have unregulated proliferation. It is unclear whether they accurately model abscission dynamics in epithelia that must regulate proliferation and differentiation during development. Using the cortical explant culture method, labeled with Sir-Tubulin, but collecting images every 15 minutes, we were able analyze the spatial and temporal dynamics of abscission in NESC midbodies

at the apical membrane. Figure 2A shows a representative NESC at an early stage of abscission, with a wide midbody. The apical (*en face*) view is the imaging plane (X-Y). When the image stack is rotated to the lateral (X-Z) view, it illustrates how the midbody bridges the two daughter cells across their cell junction, and protrudes into the ventricle. At later stages of abscission, the midbody is thinner, and sometimes a microtubule constriction site can be seen on one flank as reduced microtubule signal (Fig. 2B, arrowheads). Our time-lapse imaging can capture the steps of abscission: furrow completion, midbody formation, constriction site thinning, first abscission, and sometimes a second abscission (Fig 2C, D).

Since furrow ingression in cortical NESCs appears to be much slower than in HeLa cells (Fig 1), we predicted that abscission would also be much slower. Additionally, we wondered if abscission duration might change as brain development proceeds and NESC divisions switch from proliferative to neurogenic. To test these ideas, we measured the time from furrow initiation to first abscission in cortical NESCs at two different ages. We found that the duration was highly variable, ranging from 45 to 150 minutes, with means of 90 and 85 minutes at E11.5 and E13.5, respectively (Fig. 2E, F). Thus, while the range is wider and the average time is longer than we found in HeLa cells (68 minutes, (Janisch et al., 2018)), it is not several-fold longer like furrowing. A cumulative frequency plot shows a trend to faster abscission at the later age, when divisions are more frequently asymmetric and neurogenic (Fig 2G, solid lines). These data suggest that while the time required for abscission is roughly similar in NESCs compared to mammalian cell lines, that duration may also be developmentally regulated.

We previously found that Kif20b-depleted HeLa cells have dysregulated abscission timing, and that fixed *Kif20b* mutant brains display misshapen and disorganized midbodies. These data led to the prediction that some *Kif20b* mutant NESCs have delayed or failed abscissions. To our surprise, in live imaging, every mutant cell observed was able to complete abscission, and remarkably, the average time to first abscission was reduced by 15 minutes compared to controls at both E11.5 and E13.5 (Fig. 2E, F). Moreover, the cumulative frequency plot of *Kif20b* mutant abscissions shows similar curves at the two ages, suggesting a loss of developmental regulation (Fig 2G, dashed lines). Perhaps even more surprising, *Kif20b* mutant NESCs abscise when the midbodies are slightly wider than in controls (Fig 2 H, I). These data are puzzling because they suggest that the mutant NESCs abscise prematurely. Nevertheless, they dovetail with our previous findings in fixed samples that *Kif20b* mutant NESC midbodies tend to be wider than controls' (Janisch et al., 2013; Little and Dwyer, 2019). Together these data support the idea that Kif20b functions to coordinate abscission timing with midbody maturation. The consequences of premature abscission for cell polarity or fate are unknown.

Sequential abscissions on both midbody flanks are observable in most divisions of control and Kif20b-/- NESCs.

Next, we wanted to determine if cortical NESCs have abscission on one or both midbody flanks, the relative timing, and if this varies with developmental stage. Many studies of abscission have reported that the midbody was severed on one flank and then inherited by the daughter connected to the opposite flank (Ettinger et al., 2011;

Gromley et al., 2005; Kuo et al., 2011; Salzmann et al., 2014; Singh and Pohl, 2014). A smaller number of studies, by ourselves and others, report sequential abscissions on each flank in HeLa and MDCK cells (Gershony et al., 2017; Guizetti et al., 2011; Janisch et al., 2018). Thus, unilateral or bilateral abscission may vary with cell type, and little is known about its spatial and temporal regulation.

An attractive hypothesis is that an early symmetric proliferative division of a cortical NESC would occur through bilateral abscission and release of the midbody remnant (MBR) extracellularly, whereas a later asymmetric neurogenic division could result from unilateral abscission on one flank and midbody inheritance by the other daughter, promoting asymmetric fates. Indeed, MBRs have been found in cerebrospinal fluid of early (E10.5) mouse embryos (Dubreuil et al., 2007). However, we observed bilateral abscission just as often in E13.5 divisions as E11.5 divisions, in at least 60% of the cases (Fig. 3A, B). The two abscissions usually occurred sequentially, but occasionally took place within the same time interval. The median time between the first and second event was 30 minutes at E11.5 and 15 minutes at E13.5, with a maximum of 90 minutes (Fig. 3C, D). It is not clear whether the cases where only a single abscission could be scored with confidence were truly unilateral, or whether the second event was not detected due to imaging conditions. Further studies are needed to determine whether bilateral abscissions decrease at even later stages of corticogenesis.

We also asked whether Kif20b loss altered bilateral abscission frequency or kinetics. Surprisingly, the loss of Kif20b does not significantly alter the frequency of second abscissions (Fig. 3 A, B). It does significantly reduce the time between first and second abscissions in E11.5 NESCs by 15 minutes (Fig. 3C). In total, the time to

complete bilateral abscissions was at least 15 minutes less in the *Kif20b* mutants at both E11.5 and E13.5 (Fig. 3E, F, G). Thus, Kif20b loss does not prevent midbody release, and may in fact hasten it.

Increased association of MBRs with younger NESC division pairs undergoing proliferative divisions

The prior experiments showed that a large number of NESC midbody remnants are released at the apical membrane, an important location to impact cell fate and polarization of NESCs. The apical membranes of NESCs have primary cilia, and receive signals from the cerebrospinal fluid (Chau et al., 2015). Potentially, NESC MBRs could bind to the surfaces of neighboring cells and effect signals or be phagocytosed as seen in HeLa cells (Crowell et al., 2014). MBRs have been shown to influence proliferation or differentiation in cell lines, to influence spindle orientation in *C. elegans* embryos, and to induce ciliogenesis on MCDK cells (Bernabe-Rubio et al., 2016; Ettinger et al., 2011; Kuo et al., 2011; Singh and Pohl, 2014).

We wanted to know whether the NESC MBRs float into the ventricle, or remain associated with the apical membrane. With HeLa cell live imaging, we could follow MBR movements for > 1 hour. Unfortunately, in the live cortical explants, we were not able to follow the MBRs after the second abscission. Therefore, we used fixed cortical slabs and dissociated NESCs to study MBR disposal at different ages and types of divisions. First we determined if MBRs remain on the apical surface by immunostaining for the MBR marker citron kinase (CitK) at two ages, when either a majority of proliferative divisions (E11.5) or neurogenic divisions (E15.5) occur. Both pre-abscission midbodies

(yellow arrows) and post-abscission MBRs (white arrows) are observed at the apical membrane at both ages, suggesting that once the MBR is released it can adhere to the apical membrane (Fig. 4A, B).

To test whether midbody remnants were associated with proliferative or neurogenic NESC divisions, we modified the established NESC "pair cell" assay (methods, (Qian et al., 1998)). NESCs were dissociated from either E11.5 or E15.5 cortices, plated as single cells at clonal density in Terasaki wells, and fixed the next day to score individual NESC divisions for the presence of MBRs (Fig. 4C). Unexpectedly, we observed 30% of E11.5 division pairs had a MBR present, but only 5% of E15.5 pairs did (Fig. 4D). This striking difference suggests that E15.5 NESCs may have different regulation of either MBR release or degradation. Furthermore, Kif20b is not required for this developmental change.

These data suggest that MBRs are more associated with early proliferative divisions than later neurogenic divisions. To test this further, we scored MBR association in the different types of divisions of E11.5 NESCs. By co-labeling with NESC marker Nestin, and neuronal marker beta-III tubulin (Tubb3), the division pairs were classified as proliferative symmetric, neurogenic symmetric, and asymmetric (Figure 4E). Interestingly, E11.5 division pairs that have an associated MBR are more likely to be proliferative symmetric divisions (Fig. 4F, control). This supports the idea that MBR presence, and perhaps bilateral abscission, are associated with proliferative symmetric division. Curiously, in the *Kif20b* mutant, this association is no longer seen, perhaps due to an overall reduction of proliferative symmetric divisions (Fig. 4F, Kif20-/- bars). Thus, MBR presence may influence a NESC division towards proliferative

symmetric fates, but does not appear to be the primary effector in this process. It is not known if NESCs have similar mechanisms for MBR engulfment and degradation as other cell types (Chai et al., 2012; Crowell et al., 2014), but developmental regulation of these could change the ability of MBRs to influence NESC polarity or fates. The composition and signaling capacity of MBRs require further investigation.

Premature cell cycle exit of early Kif20b mutant NESCs may contribute to microcephaly

In the previous analyses, we noticed that *Kif20b* mutant NESCs had fewer proliferative symmetric divisions resulting in two progenitor daughters, and more neurogenic divisions with two postmitotic neuron daughters, regardless of MBR association (Fig 4F). To directly test whether *Kif20b* mutant NESCs have different division fate outcomes, we quantified the daughter fates of individual NESC divisions using the dissociated division pair assay (Figure 4E, 5A). Pooling the divisions with and without MBRs, we find that *Kif20b* mutant NESCs from E11.5 brains have a significant increase in neurogenic symmetric divisions compared to controls, 61% versus 42% (Fig 5B). This comes at the expense of fewer proliferative symmetric divisions (17% vs 38%). NESCs from older (E15.5) brains normally have more neurogenic and fewer proliferative divisions (Fig 5C, control, and Fig S1A). However, *Kif20b* mutants do not show this profound developmental shift: they always have a majority of neurogenic symmetric divisions (Fig 5C, Fig. S1B). This suggests that Kif20b's function helps bias early NESC divisions to produce two NESC daughters.

These data led to the idea that *Kif20b* mutant NESCs have premature neurogenesis (early excess cell cycle exit). To test this *in vivo,* we measured the width

of the neuronal layer at E12.5 in control and mutant cortices, when the earliest neuronal layer (preplate) is thin. Indeed, we find a small but highly significant increase in the proportional thickness of the neuronal layer of *Kif20b* mutant cortices over controls' (Figure 5D, E). This is not due to decreased neuron density (Fig. 5F). These results suggest that in early *Kif20b* mutant cortices, some daughters of NESC divisions prematurely exit the cell cycle to become postmitotic neurons, depleting the early pool of NESCs. This could contribute to the smaller brain size at birth.

We previously showed that a small percentage of NESCs in *Kif20b* mutant cortices undergo apoptosis, and that this is p53-dependent (Little and Dwyer, 2019). We further showed that p53 accumulates in the nucleus of *Kif20b* mutant NESCs at late midbody stage. Therefore, we hypothesized that the increase in symmetric neurogenic divisions (both daughters exiting the cell cycle) could also result from p53 activation. To test this, we assayed division types in *Kif20b; p53* double mutant NESCs. We modified the previous assay by feeding BrdU to higher density NESC cultures at plating, so that NESCs that divided in the dish could be identified as pairs of BrdU+ cells. Surprisingly, the increase in symmetric neurogenic divisions caused by loss of Kif20b is not prevented by p53 knockout (*Kif20b; p53* double mutants, Fig. S1D). Both the *Kif20b* mutant and *Kif20b; p53* double mutant had a 45% increase in neurogenic divisions. Cell cycle exit (BrdU+Tubb3+ cells /BrdU+ cells) was increased in NESCs double mutant for Kif20b and p53, but not p53 alone (Fig. S1E). Thus, our data show that early NESCs in the *Kif20b* mutant mouse are depleted due to both p53-dependent apoptosis (Janisch et al., 2013; Little and Dwyer, 2019) and p53-independent cell cycle exit (this paper). More

studies are needed to determine whether and how these pathways are activated by defects in midbody structure or abscission timing.

Recent progress in cell lines has elucidated a few of the signaling molecules that activate p53-mediated cell cycle arrest following mitotic delay, but abscission delay was not addressed (Lambrus et al., 2016; Meitinger et al., 2016). Furthermore, cortical NESC daughters appear to respond differently: p53 is not required for cell cycle exit (neurogenesis) following mitotic delay, but p53 does mediate apoptosis in some cells instead (Pilaz et al., 2016). This echoes the aforementioned findings in *Kif20b* mutant NESCs, but we found no evidence for delayed or defective mitosis in the *Kif20b* mutant (Janisch et al., 2013; Little and Dwyer, 2019). Since cell cycle exit is a normal developmental event for the neuronal daughters of NESCs, a non-p53 pathway may be primed to mediate it.

The cellular consequences of accelerated abscission are much less studied than those following abscission delay or failure (Stoten and Carlton, 2018). Accelerated abscission in a cell line has been induced, but no morphological or fate consequences were described (Carlton et al., 2012). Delayed abscission in HeLa cells causes persistent intercellular bridges, midbody regression/ binucleation, or cell death (Gromley et al., 2003). By contrast, delayed abscission timing in the fly germline is important for maintaining stem cell fate (Lenhart and DiNardo, 2015). In cortical neuroepithelium, other signaling-related events happening concurrently with abscission at the apical membrane could be affected by the duration or timing of abscission. These include new apical junction formation, notch signaling across the junction, and centrosome docking/ ciliogenesis, which are all known to influence cell fate. In addition, the MBRs released

from NESC divisions may function to sequester or transmit fate determinants. Future work in multiple cell types is needed to compare the signaling pathways affected, and cellular and developmental consequences of delayed versus accelerated abscissions.

Methods

Mice

The mouse protocols are approved by the IACUC and the colonies are maintained in accordance with NIH guidelines. The morning of the vaginal plug was considered E0.5. All embryos were harvested by cesarean section and littermate controls were used when possible. The *Kif20b*^{magoo} (*Kif20b*$^{-/-}$) mutant mouse was generated in an ENU screen (Dwyer et al. 2011). It carries a loss-of-function splice site mutation that reduces the protein to undetectable levels (Janisch et al., 2013). The *Kif20b* mutant mouse was crossed with both the mT/mG reporter line (Jax stock #007576) and Sox2-Cre mice (JAX stock #008454) (Hayashi et al., 2002; Muzumdar et al., 2007) to produce mice that expressed membrane-localized GFP. The p53 null mouse (Trp53^{tm1Tyj} (JAX stock #002101) was crossed to the *Kif20b* mutant mouse (Jacks et al., 1994; Little and Dwyer, 2019).

Antibodies and immunofluorescence staining

Following fixation, cortical slabs or NESC cultures were incubated for an hour at room temperature in blocking buffer (0.1% Triton-X, 2% Normal Goat Serum in PBS) and then overnight at 4 °C or for three hours at room temperature in the appropriate primary antibody solution (antibody diluted in blocking solution). After primary incubation, coverslips were rinsed in PBS (3 times every 10 min) or slabs were rinsed in PBS-triton

once followed by two PBS rinses and then incubated at room temperature with appropriate secondary antibody solution (1:200 dilution) for 30 min (cultures) or 45 mins (slabs) in the dark. Following final washes in PBS, coverslips were mounted onto glass slides with Fluoromount (Vectashield, 4-1000) or slabs with flurogel (Electron Microscopy Sciences 17985-10). Antibodies used: Nestin (Aves Lab, NES), Tubb3 (TUJ1, Abcam rabbit 52623, Biolegend mouse 801201), Criton kinase (CITK) (BD Biosciences 611376), Aurora B (Abcam ab2254), Zonula occludens (Zo-1) (DSHB R26.4DC), BrdU (BD Biosciences 347580).

Pair cell assay and NESC cultures

The pair cell assay for dissociated cortical NESC divisions was adapted from ((Chau et al., 2015; Qian et al., 1998)) E11.5, E12.5 or E15.5 mouse embryos were dissected from the dam in hibernate media (Gibco Hibernate-E A12476-01). Cortices were removed and placed into a 15mL conical tube. Meninges were removed from E15.5 cortices. Papain from Worthington kit (Worthington Biochemical Corporation, LK003150) was used for dissociation. Cortices were placed on a rotator at 37°C for 30 mins (E11.5 or E12) or 45 mins (E15). Manual dissociation followed by centrifugation at 4C at 1300 rpm for 10 minutes and then wash with DMEM (Invitrogen 11960-051). The wash and centrifugation are repeated three times. After the final wash, the cortices were manually dissociated with a 1 mL pipette followed by a glass Pasteur pipette. The tissue was resuspended in final culture media (resuspension volume varied by age and size of cortices). Final culture media is base media filtered with 0.22 μm cellulose acetate membrane (BD Biosciences 302995) with 100μl of N2 (Invitrogen Cat. No. 17502-048) and 100 μl N-acetyl-cysteine (Sigma Cat No A-9165), and 20 μl of bFGF (Invitrogen

Cat. No. 13256-029) per 20 mL. Base media is DMEM with 2mL Na-Pyruvate (Invitrogen 11360–070), 2mL L-glutamine (Gibco A2916801), 4mL 50X B-27 without Vitamin B (Gibco 12587010) per 200mL of DMEM. The cortices were at room temperature for 15 minutes to allow for the clumps to settle to the bottom of the conical tube. Between 1 to 3 µl of cells from the top of the tube were added to each well of the poly-L-lysine coated Terasaki plates (Fisher cat # 07-000-401) to get a low density. The plates were placed in a humidifying chamber and into a 37°C incubator with 5% CO2 to incubate for 20 hours. NESC cultures were fixed with 4% paraformaldehyde (PFA) for 2 minutes followed by 5 minutes cold methanol. Immunostaining was followed as described above except the plate was kept in a humidified chamber to prevent evaporation and volumes of washes and antibodies were adjusted. All washes were done by flooding the plate with 5mL of PBS. Primary and secondary incubations were done by adding 10µl of solution to each well.

Images were acquired using a Zeiss AxioZoom Observer.Z1 with a 40x air objective.

BrdU in a modified pair cell assay

Primary cortical NESCs were plated on coverslips at 100,000 cell density with 10uM BrdU (Sigma B5002-500mg) and allowed to incubate at 37°C for 6 hours. The media was exchanged to wash out the BrdU, and the culture continued to incubate for 14hrs. The cells were then fixed at 20 hours with 4% PFA for 10 minutes. Antigen retrieval was performed using 0.07M NaOH for 2 minutes before proceeding to immunostaining. Images were acquired at 40x using a Zeiss AxioImagerZ1 microscope with AxioCam mRM.

Cortical slabs for fixed tissue

This method was previously described (Janisch and Dwyer, 2016). Briefly, the skulls were opened to reveal the cortices. The entire head was fixed for 20 minutes in 2% PFA for E11.5 and 4% PFA for E15.5. Cortices were pinched off and placed in slide wells (Cat # 70366-12, 70366-13). The total slab thickness varied by age (E11.5: ~150μm, E15.5: ~400μm). The slabs were briefly fixed again with PFA before immunostaining. Images were acquired using the 60x objective on the Applied Precision (GE) DeltaVision microscope.

Cortical slabs for cleavage furrow and abscission live imaging

E11.5 or E13.5 embryos were removed from the uterus and dissected in cold 1xPBS. Embryos were checked for GFP or RFP fluorescence before removal of cortices. The embryos heads were removed followed by the opening of the skull. Once the skull had been opened tweezers were used to pinch out the cortices. Each cortex was placed into a glass bottom dish (MatTek P35G-1.0-20-C) with 50nM silicone-rhodamine tubulin (SirTubulin) (Cytoskeleton CY-SC002) made in final culture media. The slabs were then trimmed and flipped, so the apical surface was facing towards the glass coverslip. Each dish was placed in a humidifying chamber and into a 37°C incubator with 5% CO2 overnight (Approximately 15 hours). The next day the cortices were removed from the incubator, and the 50nM Sir-Tubulin-containing media was removed. Matrigel (Corning 356237) (1:3 dilution in final culture media) was added to the cortical slab. High vacuum grease (Fisher 14-635-5D) was placed on the edge of the glass coverslip, and a coverslip (Fisher 12-545-100) was placed over the top of the slab. Gentle pressure was applied to the coverslip at the spots where the vacuum grease was placed. The slabs were placed back into the incubator, and the Matrigel was allowed to solidify for 5

minutes. Final culture media was added to the dish, and then imaging was performed. An Applied Precision (GE) DeltaVision with Truelight Deconvolution and softWorx suite 5.5 image acquisition software equipped with a heating plate and 40X objective was used for time-lapse image acquisition. Images were taken every 15 minutes for abscission and every 3 minutes for cleavage furrowing for up to 6 hours. Z steps were 0.4μm, and approximately 10 μm of the cortical slab was imaged. The total slab thickness varied by age (E11.5: ~150μm, E13.5: ~200μm).

Abscission and cleavage furrow analysis

Deconvolved full-z-stacks and maximum intensity projection images were analyzed using ImageJ. The time zero was the last time point before furrow initiation and determined using the membrane channel. The formation of the midbody was followed using the SiR-Tubulin channel. Abscission was determined as the time point where there was complete removal of tubulin on one or both sides of the midbody bulge. The width of the midbody was measured at the time point before abscission and was measured on the side of the midbody bulge in which abscission occurs. For cleavage furrowing, the length and width of the cell were measured from the time point right before the first ingression of the membrane started. This measurement was done at every time point until there was no longer any separation between the two sides of the furrow. Furrowing was then determined to be completed. Images for 3-D renderings were acquired using higher resolution (40x objective, 0.2μm z-step) image stacks on E13.5 cortical slabs incubated in 200nM SiR-Tubulin. 3-D renderings were created in Volocity (access to Volocity kindly provided by Dr. Barry Hinton).

Statistical analysis

All data and statistical analysis were performed with Excel (Microsoft) and GraphPad Prism. Data was tested for normality. All statistical tests were identified in the corresponding figure legends.

Acknowledgments

This work was supported by National Institutes of Health (R01 NS076640 and R21 NS106162 to N.D.D.) and the 2018 Robert R. Wagner Fellowship to K.C.M. The authors would like to thank Xiaowei Lu, Bettina Winckler, Ann Sutherland for breeders and advice on mTmG and Sox2-cre mice, Sarah Siegrist, Jung-Bum Shin, Ahna Skop and their labs for advice and discussion. The authors would like to thank Maria Lehtinen and Anthony Lamantia for pair cell assay protocols and advice. The authors would like to thank Sara Martin and Adriana Ehlers for their help with data analysis.

Author Contributions

K.C.M conceptualized the experiments, performed data curation for Figures 1-5 and Supplementary Figure 1 A-B, wrote the original draft, and participated in the review and editing of the manuscript. J.N.L performed data curation for Supplementary Figure1 C-E. N.D.D conceptualized the experiments and reviewed and edited the manuscript.

References

Abaza, A., J.M. Soleilhac, J. Westendorf, M. Piel, I. Crevel, A. Roux, and F. Pirollet. 2003. M phase phosphoprotein 1 is a human plus-end-directed kinesin-related protein required for cytokinesis. *J Biol Chem*. 278:27844-27852.

Bernabe-Rubio, M., G. Andres, J. Casares-Arias, J. Fernandez-Barrera, L. Rangel, N. Reglero-Real, D.C. Gershlick, J.J. Fernandez, J. Millan, I. Correas, D.G. Miguez, and M.A.

Alonso. 2016. Novel role for the midbody in primary ciliogenesis by polarized epithelial cells. *The Journal of cell biology*. 214:259-273.

Bizzotto, S., and F. Francis. 2015. Morphological and functional aspects of progenitors perturbed in cortical malformations. *Frontiers in cellular neuroscience*. 9:30.

Bondeson, M.L., K. Ericson, S. Gudmundsson, A. Ameur, F. Ponten, J. Wesstrom, C. Frykholm, and M. Wilbe. 2017. A nonsense mutation in CEP55 defines a new locus for a Meckel-like syndrome, an autosomal recessive lethal fetal ciliopathy. *Clin Genet*.

Carlton, J.G., A. Caballe, M. Agromayor, M. Kloc, and J. Martin-Serrano. 2012. ESCRT-III governs the Aurora B-mediated abscission checkpoint through CHMP4C. *Science*. 336:220-225.

Chai, Y., D. Tian, Y. Yang, G. Feng, Z. Cheng, W. Li, and G. Ou. 2012. Apoptotic regulators promote cytokinetic midbody degradation in C. elegans. *The Journal of cell biology*. 199:1047-1055.

Chau, K.F., M.W. Springel, K.G. Broadbelt, H.Y. Park, S. Topal, M.P. Lun, H. Mullan, T. Maynard, H. Steen, A.S. LaMantia, and M.K. Lehtinen. 2015. Progressive Differentiation and Instructive Capacities of Amniotic Fluid and Cerebrospinal Fluid Proteomes following Neural Tube Closure. *Dev Cell*. 35:789-802.

Connell, J.W., C. Lindon, J.P. Luzio, and E. Reid. 2009. Spastin couples microtubule severing to membrane traffic in completion of cytokinesis and secretion. *Traffic*. 10:42-56.

Crowell, E.F., A.L. Gaffuri, B. Gayraud-Morel, S. Tajbakhsh, and A. Echard. 2014. Engulfment of the midbody remnant after cytokinesis in mammalian cells. *J Cell Sci*. 127:3840-3851.

Di Cunto, F., S. Imarisio, E. Hirsch, V. Broccoli, A. Bulfone, A. Migheli, C. Atzori, E. Turco, R. Triolo, G.P. Dotto, L. Silengo, and F. Altruda. 2000. Defective neurogenesis in citron kinase knockout mice by altered cytokinesis and massive apoptosis. *Neuron*. 28:115-127.

Dionne, L.K., X.J. Wang, and R. Prekeris. 2015. Midbody: from cellular junk to regulator of cell polarity and cell fate. *Curr Opin Cell Biol*. 35:51-58.

Dubreuil, V., A.M. Marzesco, D. Corbeil, W.B. Huttner, and M. Wilsch-Brauninger. 2007. Midbody and primary cilium of neural progenitors release extracellular membrane particles enriched in the stem cell marker prominin-1. *The Journal of cell biology*. 176:483-495.

Dwyer, N.D., B. Chen, S.J. Chou, S. Hippenmeyer, L. Nguyen, and H.T. Ghashghaei. 2016. Neural Stem Cells to Cerebral Cortex: Emerging Mechanisms Regulating Progenitor Behavior and Productivity. *J Neurosci*. 36:11394-11401.

Dwyer, N.D., D.K. Manning, J.L. Moran, R. Mudbhary, M.S. Fleming, C.B. Favero, V.M. Vock, D.D. O'Leary, C.A. Walsh, and D.R. Beier. 2011. A forward genetic screen with a thalamocortical axon reporter mouse yields novel neurodevelopment mutants and a distinct Emx2 mutant phenotype. *Neural Dev*. 6:3.

Ettinger, A.W., M. Wilsch-Brauninger, A.M. Marzesco, M. Bickle, A. Lohmann, Z. Maliga, J. Karbanova, D. Corbeil, A.A. Hyman, and W.B. Huttner. 2011. Proliferating versus differentiating stem and cancer cells exhibit distinct midbody-release behaviour. *Nat Commun*. 2:503.

Frosk, P., H.H. Arts, J. Philippe, C.S. Gunn, E.L. Brown, B. Chodirker, L. Simard, J. Majewski, S. Fahiminiya, C. Russell, Y.P. Liu, F.C. Consortium, M. Canadian Rare Diseases, N. Mechanisms, R. Hegele, N. Katsanis, C. Goerz, M.R. Del Bigio, and E.E. Davis. 2017. A truncating mutation in CEP55 is the likely cause of MARCH, a novel syndrome affecting neuronal mitosis. *J Med Genet*. 54:490-501.

Gershony, O., S. Sherman, S. Adar, I. Segal, D. Nachmias, I. Goliand, and N. Elia. 2017. Measuring abscission spatiotemporal dynamics using quantitative high-resolution microscopy. *Methods in cell biology*. 137:205-224.

Green, R.A., E. Paluch, and K. Oegema. 2012. Cytokinesis in animal cells. *Annu Rev Cell Dev Biol*. 28:29-58.

Gromley, A., A. Jurczyk, J. Sillibourne, E. Halilovic, M. Mogensen, I. Groisman, M. Blomberg, and S. Doxsey. 2003. A novel human protein of the maternal centriole is required for the final stages of cytokinesis and entry into S phase. *The Journal of cell biology*. 161:535-545.

Gromley, A., C. Yeaman, J. Rosa, S. Redick, C.T. Chen, S. Mirabelle, M. Guha, J. Sillibourne, and S.J. Doxsey. 2005. Centriolin anchoring of exocyst and SNARE complexes at the midbody is required for secretory-vesicle-mediated abscission. *Cell*. 123:75-87.

Guizetti, J., L. Schermelleh, J. Mantler, S. Maar, I. Poser, H. Leonhardt, T. Muller-Reichert, and D.W. Gerlich. 2011. Cortical constriction during abscission involves helices of ESCRT-III-dependent filaments. *Science*. 331:1616-1620.

Hayashi, S., P. Lewis, L. Pevny, and A.P. McMahon. 2002. Efficient gene modulation in mouse epiblast using a Sox2Cre transgenic mouse strain. *Mech Dev*. 119 Suppl 1:S97-S101.

Higashi, T., T.R. Arnold, R.E. Stephenson, K.M. Dinshaw, and A.L. Miller. 2016. Maintenance of the Epithelial Barrier and Remodeling of Cell-Cell Junctions during Cytokinesis. *Curr Biol*. 26:1829-1842.

Jacks, T., L. Remington, B.O. Williams, E.M. Schmitt, S. Halachmi, R.T. Bronson, and R.A. Weinberg. 1994. Tumor spectrum analysis in p53-mutant mice. *Curr Biol*. 4:1-7.

Janisch, K.M., and N.D. Dwyer. 2016. Imaging and quantitative analysis of cytokinesis in developing brains of Kinesin-6 mutant mice. *Methods in cell biology*. 131:233-252.

Janisch, K.M., K.C. McNeely, J.M. Dardick, S.H. Lim, and N.D. Dwyer. 2018. Kinesin-6 KIF20B is required for efficient cytokinetic furrowing and timely abscission in human cells. *Mol Biol Cell*. 29:166-179.

Janisch, K.M., V.M. Vock, M.S. Fleming, A. Shrestha, C.M. Grimsley-Myers, B.A. Rasoul, S.A. Neale, T.D. Cupp, J.M. Kinchen, K.F. Liem, Jr., and N.D. Dwyer. 2013. The vertebrate-specific Kinesin-6, Kif20b, is required for normal cytokinesis of polarized cortical stem cells and cerebral cortex size. *Development*. 140:4672-4682.

Kim, S., M.K. Lehtinen, A. Sessa, M.W. Zappaterra, S.H. Cho, D. Gonzalez, B. Boggan, C.A. Austin, J. Wijnholds, M.J. Gambello, J. Malicki, A.S. LaMantia, V. Broccoli, and C.A. Walsh. 2010. The apical complex couples cell fate and cell survival to cerebral cortical development. *Neuron*. 66:69-84.

Kuo, T.C., C.T. Chen, D. Baron, T.T. Onder, S. Loewer, S. Almeida, C.M. Weismann, P. Xu, J.M. Houghton, F.B. Gao, G.Q. Daley, and S. Doxsey. 2011. Midbody accumulation through evasion of autophagy contributes to cellular reprogramming and tumorigenicity. *Nat Cell Biol*. 13:1214-1223.

Lambrus, B.G., V. Daggubati, Y. Uetake, P.M. Scott, K.M. Clutario, G. Sluder, and A.J. Holland. 2016. A USP28-53BP1-p53-p21 signaling axis arrests growth after centrosome loss or prolonged mitosis. *The Journal of cell biology*. 214:143-153.

Lenhart, K.F., and S. DiNardo. 2015. Somatic cell encystment promotes abscission in germline stem cells following a regulated block in cytokinesis. *Dev Cell*. 34:192-205.

Li, H., S.L. Bielas, M.S. Zaki, S. Ismail, D. Farfara, K. Um, R.O. Rosti, E.C. Scott, S. Tu, N.C. Chi, S. Gabriel, E.Z. Erson-Omay, A.G. Ercan-Sencicek, K. Yasuno, A.O. Caglayan, H.

Kaymakcalan, B. Ekici, K. Bilguvar, M. Gunel, and J.G. Gleeson. 2016. Biallelic Mutations in Citron Kinase Link Mitotic Cytokinesis to Human Primary Microcephaly. *Am J Hum Genet*. 99:501-510.

Little, J.N., and N.D. Dwyer. 2019. p53 deletion rescues lethal microcephaly in a mouse model with neural stem cell abscission defects. *Hum Mol Genet*. 28:434-447.

Meitinger, F., J.V. Anzola, M. Kaulich, A. Richardson, J.D. Stender, C. Benner, C.K. Glass, S.F. Dowdy, A. Desai, A.K. Shiau, and K. Oegema. 2016. 53BP1 and USP28 mediate p53 activation and G1 arrest after centrosome loss or extended mitotic duration. *The Journal of cell biology*. 214:155-166.

Mierzwa, B., and D.W. Gerlich. 2014. Cytokinetic abscission: molecular mechanisms and temporal control. *Dev Cell*. 31:525-538.

Muzumdar, M.D., B. Tasic, K. Miyamichi, L. Li, and L. Luo. 2007. A global double-fluorescent Cre reporter mouse. *Genesis*. 45:593-605.

Nahse, V., L. Christ, H. Stenmark, and C. Campsteijn. 2017. The Abscission Checkpoint: Making It to the Final Cut. *Trends Cell Biol*. 27:1-11.

Paridaen, J.T., and W.B. Huttner. 2014. Neurogenesis during development of the vertebrate central nervous system. *EMBO Rep*. 15:351-364.

Pilaz, L.J., J.J. McMahon, E.E. Miller, A.L. Lennox, A. Suzuki, E. Salmon, and D.L. Silver. 2016. Prolonged Mitosis of Neural Progenitors Alters Cell Fate in the Developing Brain. *Neuron*. 89:83-99.

Pollarolo, G., J.G. Schulz, S. Munck, and C.G. Dotti. 2011. Cytokinesis remnants define first neuronal asymmetry in vivo. *Nat Neurosci*. 14:1525-1533.

Qian, X., S.K. Goderie, Q. Shen, J.H. Stern, and S. Temple. 1998. Intrinsic programs of patterned cell lineages in isolated vertebrate CNS ventricular zone cells. *Development*. 125:3143-3152.

Salzmann, V., C. Chen, C.Y. Chiang, A. Tiyaboonchai, M. Mayer, and Y.M. Yamashita. 2014. Centrosome-dependent asymmetric inheritance of the midbody ring in Drosophila germline stem cell division. *Mol Biol Cell*. 25:267-275.

Singh, D., and C. Pohl. 2014. A function for the midbody remnant in embryonic patterning. *Commun Integr Biol*. 7:e28533.

Skop, A.R., H. Liu, J. Yates, 3rd, B.J. Meyer, and R. Heald. 2004. Dissection of the mammalian midbody proteome reveals conserved cytokinesis mechanisms. *Science*. 305:61-66.

Stoten, C.L., and J.G. Carlton. 2018. ESCRT-dependent control of membrane remodelling during cell division. *Semin Cell Dev Biol*. 74:50-65.

Figure 1: Asymmetric furrow ingression is smooth but relatively slow in embryonic cortical neuroepithelium of both control and *Kif20b* mutants.

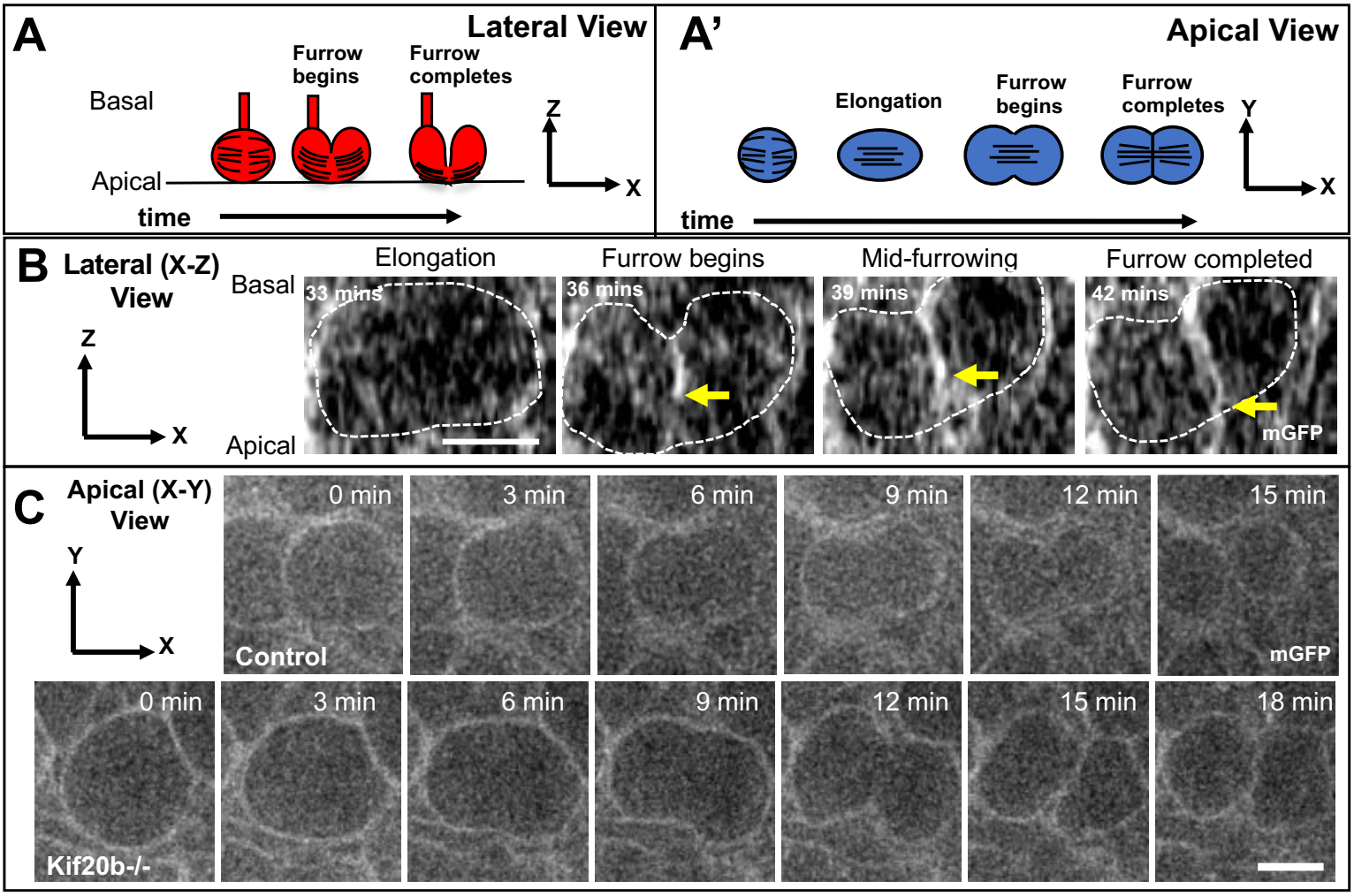

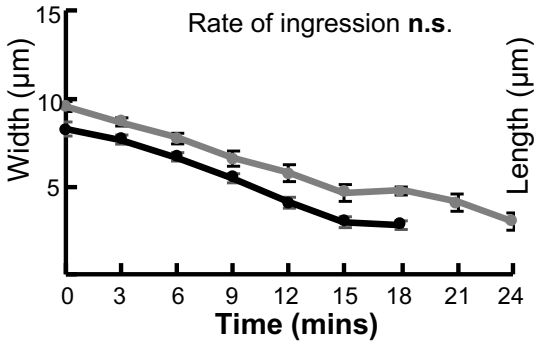

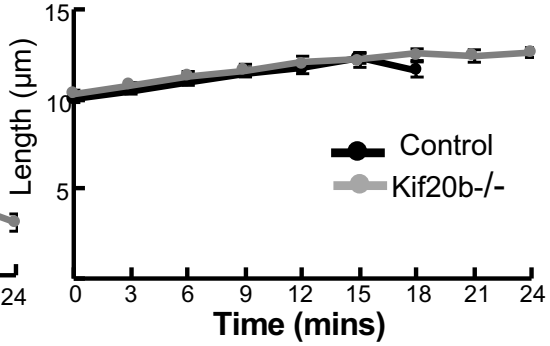

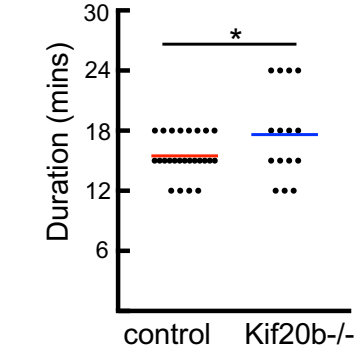

Figure 1: Asymmetric furrow ingression is smooth but relatively slow in embryonic cortical neuroepithelium of both control and *Kif20b* mutants.
(A, A') Schematic diagrams of asymmetric cytokinetic furrow ingression of cortical neuroepithelial stem cells (NESCs) as viewed from a lateral or apical (*en face*) perspective.
(B) Asymmetric cleavage furrow ingression is imaged in an E13.5 cortical slab explant of a mouse embryo expressing transgenic membrane-GFP (GFP shown as white). Example of an NESC furrowing from basal to apical (yellow arrows indicate depth of furrow). "Lateral" view (x-z) is rotated orthogonally from the imaging plane (x-y).
(C) Representative time-lapse series of basolateral furrow ingression in control and *Kif20b* mutant (-/-) NESCs. Time zero is the last time point before furrowing begins.
(D) Furrow width plotted over time shows ingression proceeds smoothly at the same slow rate (0.4 μm/min) in both control and *Kif20b-/-* cells.
(E) Pole to pole elongation over time was similar in control and *Kif20b-/-* cells.
(F) Average time to furrow completion was increased in the *Kif20b-/-* mutants due to larger starting width but same rate of ingression.
n=25 control cells from 3 brains (2 +/- and 1 +/+), and 15 *Kif20b-/-* cells from 2 brains. Scale bars, 5μm.
* $p<0.05$: Student's t-test; n.s. not significant.

Figure 2: Apical abscission in cortical neuroepithelium is variable in duration but accelerated in *Kif20b* mutants.

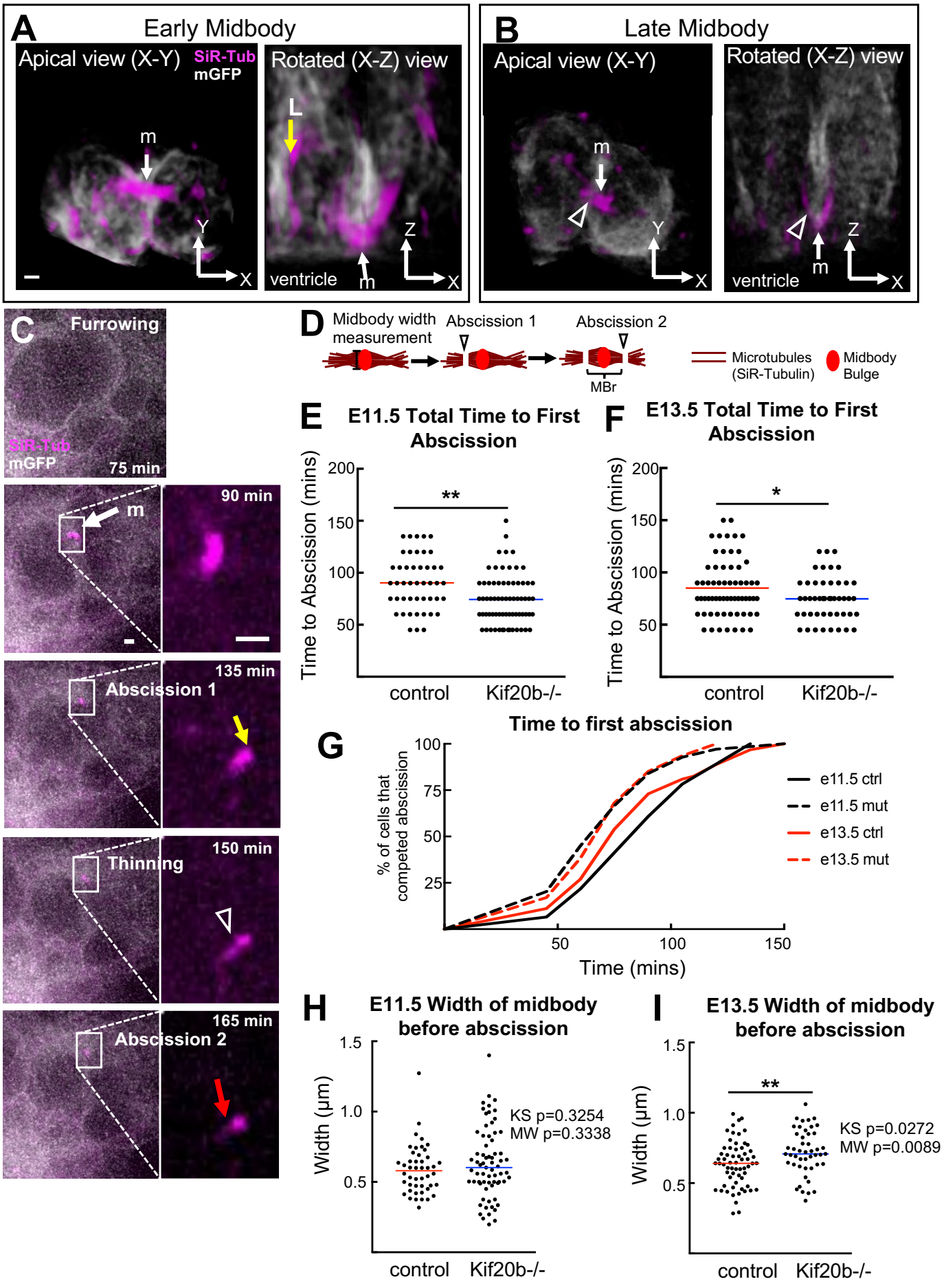

Figure 2: Apical abscission in cortical neuroepithelium is variable in duration but accelerated in *Kif20b* mutants.

Embryonic cortical explants from membrane-GFP transgenic mice (GFP shown as white) were labeled with SiR-Tubulin (magenta) and image stacks collected every 15 minutes. Note that this plasma membrane-targeted GFP localizes to the plasma membrane of the furrow but not the midbody.

(A, B) 3D renderings of representative cells at early and late midbody stages from both the apical view and rotated lateral view show midbodies (m, arrow) form at the apical membrane (ventricular surface). Late midbody is thinner with constriction site on one flank (arrowhead). L, longitudinal microtubules.

(C) Representative cortical NESC undergoing abscission. Left side, whole cell; right side, zoom of boxed midbody region. Discernible steps include: midbody formation (m, white arrow), first abscission (yellow arrow), constriction site thinning (white arrowhead) and second abscission (red arrow).

(D) Schematic showing how abscission timing was scored and midbody width measured using SiR-Tubulin labeling.

(E, F) Time to first abscission was scored in control and *Kif20b* mutant NESCs in both E11.5 and E13.5 explants. Time zero is the last time point before furrowing begins. Red and blue lines indicate means.

(G) Cumulative frequency graph shows shift to shorter abscission durations in controls between E11.5 and E13.5 (solid lines), and in *Kif20b* mutants NESCs at both ages (dashed lines).

(H, I) Width of the midbody was measured at the time point right before the 1st abscission at both E11.5 (H) and E13.5 (I). Red and blue lines indicate medians.

For E11.5, n= 46 control cells (from 4 +/+ brains); 69 *Kif20b*-/- cells (4 brains). For E13.5, n= 63 control cells (5 +/+ brains); 47 *Kif20b*-/- cells (3 brains).

**p<0.01, *p<0.05: Student's t-test for E and F; Kolmogorov–Smirnov (K-S) and Mann-Whitney (M-W) tests for H and I. Scale bars,1 μm.

Figure 3: Sequential bilateral abscissions are observed in most NESC divisions, and occur faster in *Kif20b* mutant brains.

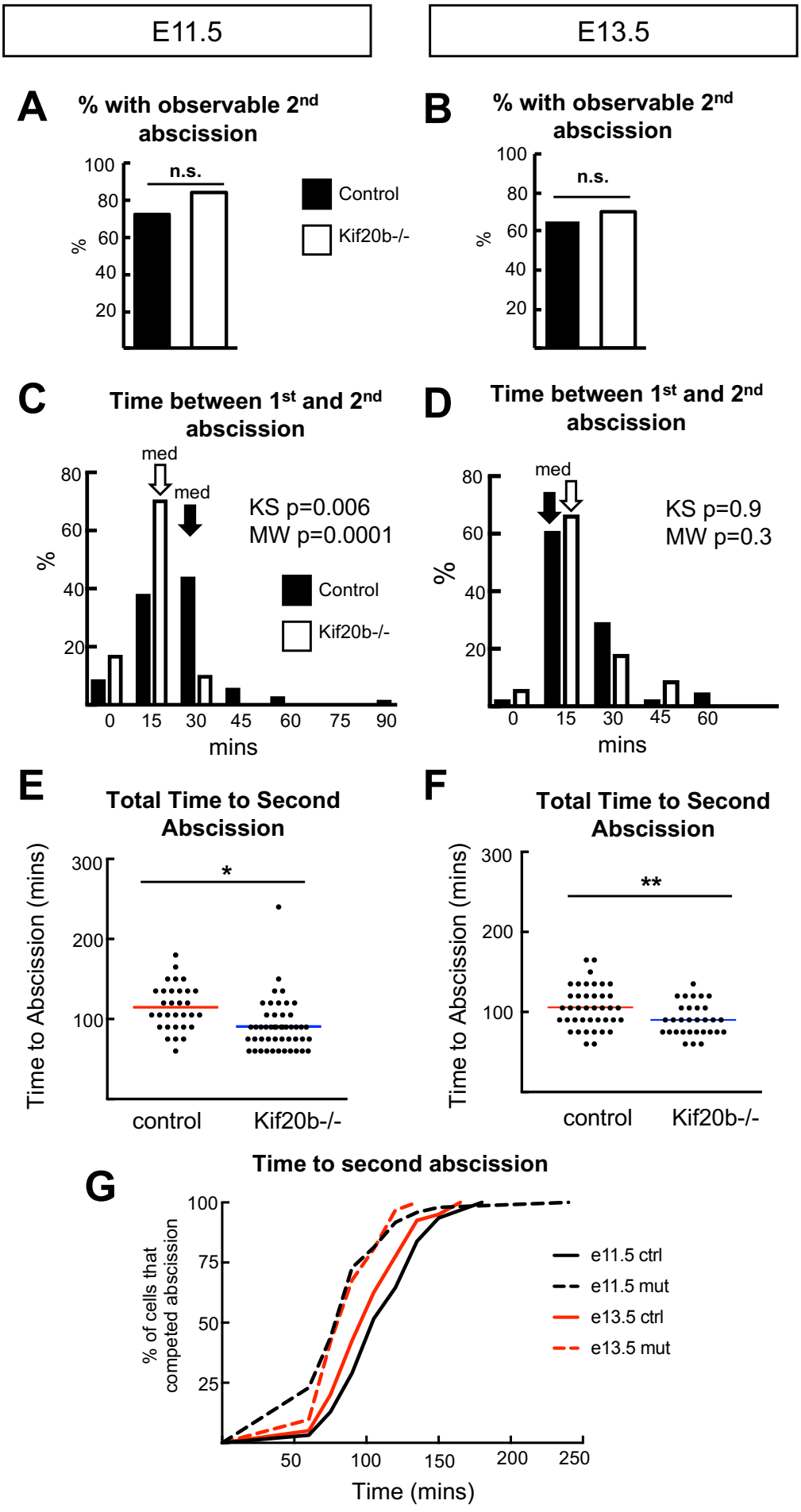

Figure 3: Sequential bilateral abscissions are observed in most NESC divisions, and occur faster in *Kif20b* mutant brains.
(A, B) In both E11.5 and E13.5 brains, the 2nd abscission event was observable in more than 60% of cases, regardless of genotype.
(C, D) The second abscission was usually detected within 30 minutes of the first abscission, but was within 15 minutes in *Kif20b* mutant cells at E11.5.
(E, F) The total time for bilateral abscissions is reduced in *Kif20b* mutants at both ages. Red and blue lines indicate means.
(G) Cumulative frequency graph shows the total time to complete bilateral abscissions is slightly reduced in E13.5 control brains compared to E11.5, and at both ages in *Kif20b* mutant brains.
For E11.5, n= 34 control (4 +/+ brains); 56 *Kif20b-/-* cells (4 brains). For E13.5, n= 40 control (5 +/+ brains), 30 *Kif20b-/-* cells (3 brains).
**p<0.01, *p<0.05, n.s. not significant: Fisher's Exact test for A and B; Kolmogorov–Smirnov (K-S) and Mann-Whitney (M-W) tests for C and D; Student's t-test for E and F.

Figure 4: Post-abscission midbody remnants (MBR) are detected at the apical membrane, and associated with early proliferative symmetric divisions.

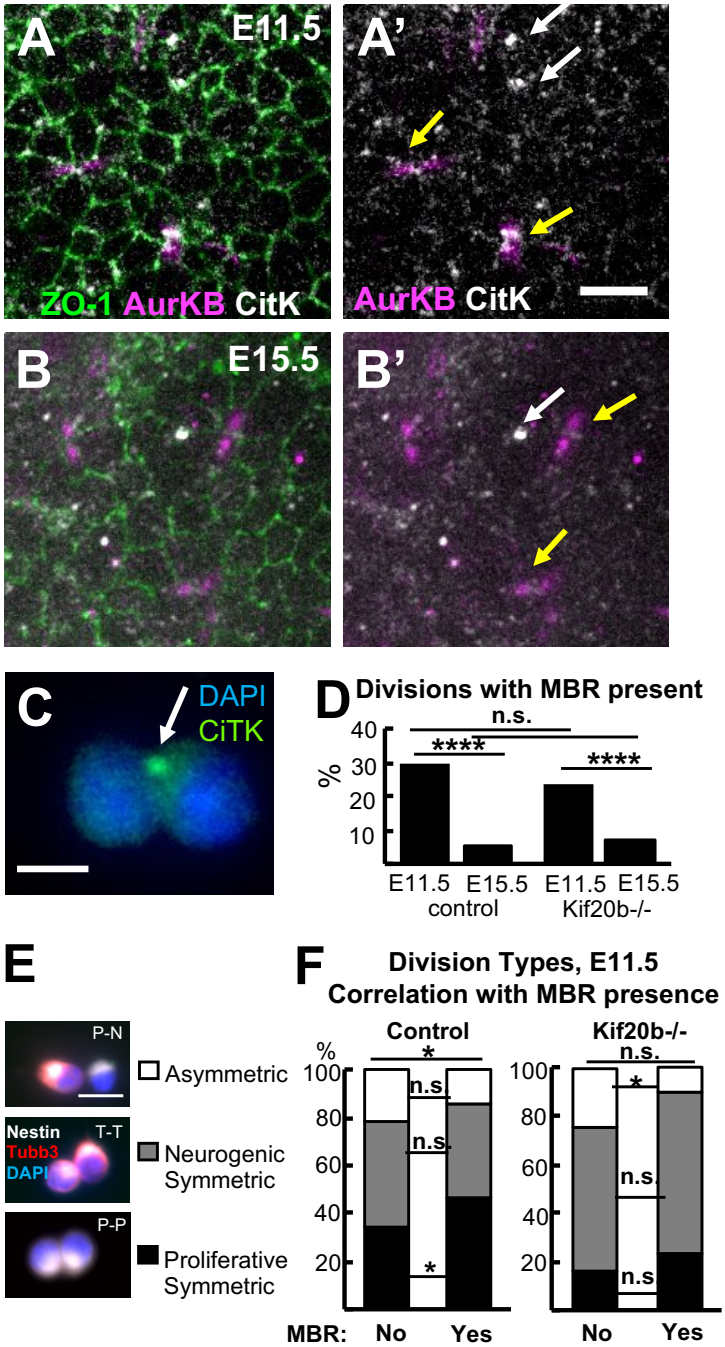

Figure 4: Post-abscission midbody remnants (MBR) are detected at the apical membrane, and associated with early proliferative symmetric divisions.

(A, B) Images of apical membrane of E11.5 or E15.5 cortical slabs show post-abscission MBRs (white arrows), as well as pre-abscission midbodies (yellow arrows), by immunostaining for endogenous markers zonula occludens (ZO-1, apical junctions, green), aurora kinase B (AurKB, MB flanks, pink), and citron kinase (CitK, MB bulge, white).

(C) Example of a dissociated E11.5 NESC that divided *in vitro*. The pair of daughter cells has an associated MBR labeled by CitK (arrow).

(D) E11.5 NESC division pairs are much more likely to have a MBR present than E15.5 division pairs, and this difference does not depend on Kif20b.

(E) Examples of the three different division types detected using the stem cell marker Nestin, and the neuronal marker, Tubb3. P, progenitor (Nestin+); N, neuron (Tubb3+); T, transitional neuron (Nestin+, Tubb3+).

(F) The proportions of division types were compared in pairs with or without a MBR. Control NESC division pairs show a correlation between MBRs and proliferative divisions, but *Kif20b* mutant NESCs do not.

For E11.5, n= 394 control (3 +/- and 2 +/+ brains) and 272 *Kif20b*-/- divisions (4 brains). For E15.5, n= 241 control (4 +/- and 1 +/+ brains) and 280 *Kif20b*-/- divisions (5 brains). ****p<0.0001, ***p<0.001, **p<0.01, *p<0.05, n.s. not significant: Fisher's exact test in D; chi-square test for the population and Fisher's Exact test for individual groups in F. Scale bars, 5μm.

Figure 5: Loss of Kif20b is associated with reduced proliferative symmetric divisions and increased neuronal daughter cells in early corticogenesis.

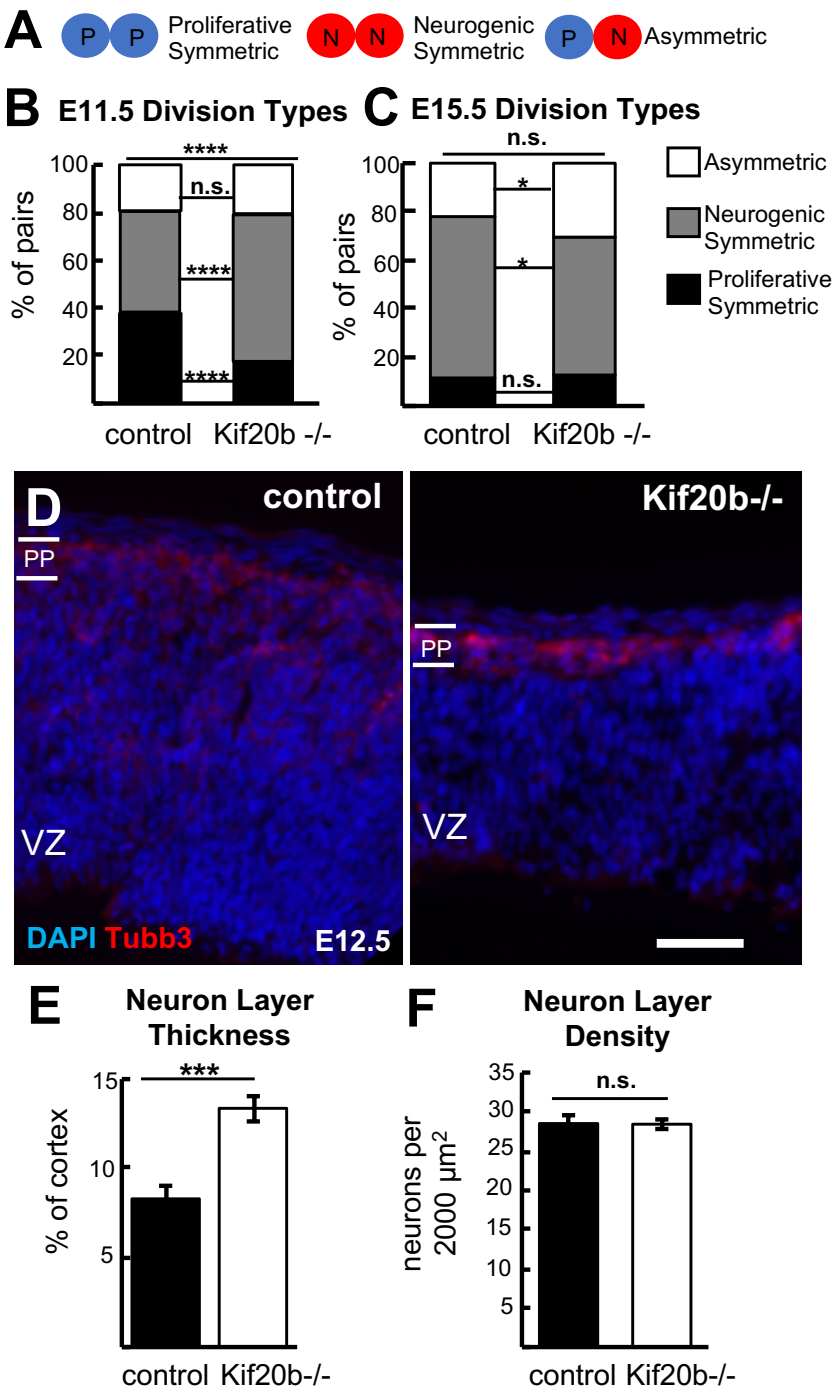

Figure 5: Loss of Kif20b is associated with reduced proliferative symmetric divisions and increased neuronal daughter cells in early corticogenesis.
(A) Schematic of the three different division types in dissociated NESCs, assayed as in Fig 4E.
(B, C) *Kif20b* -/- NESCs have less than half the percentage of proliferative symmetric divisions as controls at E11.5, with a concomitant increase in neurogenic symmetric divisions. E15.5 NESCs show similar percentages in control and *Kif20b* mutant.
For E11.5, n= 394 control (3 +/- and 2 +/+ brains) and 272 *Kif20b-/-* divisions (4 brains). For E15.5, n= 241 control (4 +/- and 1 +/+ brains) and 280 *Kif20b-/-* divisions (5 brains).
(D) Representative images of E12.5 cortical sections from control and *Kif20b*-/- brains, with staining for neuronal tubulin (Tubb3, red) and DAPI, showing the nascent neuronal layer (preplate, pp) above the stem cell layer (ventricular zone, vz). These neurons were born from NESC divisions at E11.5 and migrated up to the preplate. Scale bar 50μm.
(E) The proportional thickness of the E12.5 neuronal layer is increased in the *Kif20b* mutant brains, suggesting premature neurogenesis.
(F) There is no significant difference in neuronal density in the preplate of *Kif20b* mutants at E12.5. N= 6 control (+/+), 5 mutant (-/-) brains.
****p<0.0001, ***p<0.001, **p<0.01, *p<0.05, n.s. not significant; chi-square test for the population and Fisher's exact test for individual groups in B and C; Student's t-test for E and F.

Supplemental Figure 1: The increased neuronal fate of *Kif20b* mutant NESC daughters during early cortical development is not p53-dependent.

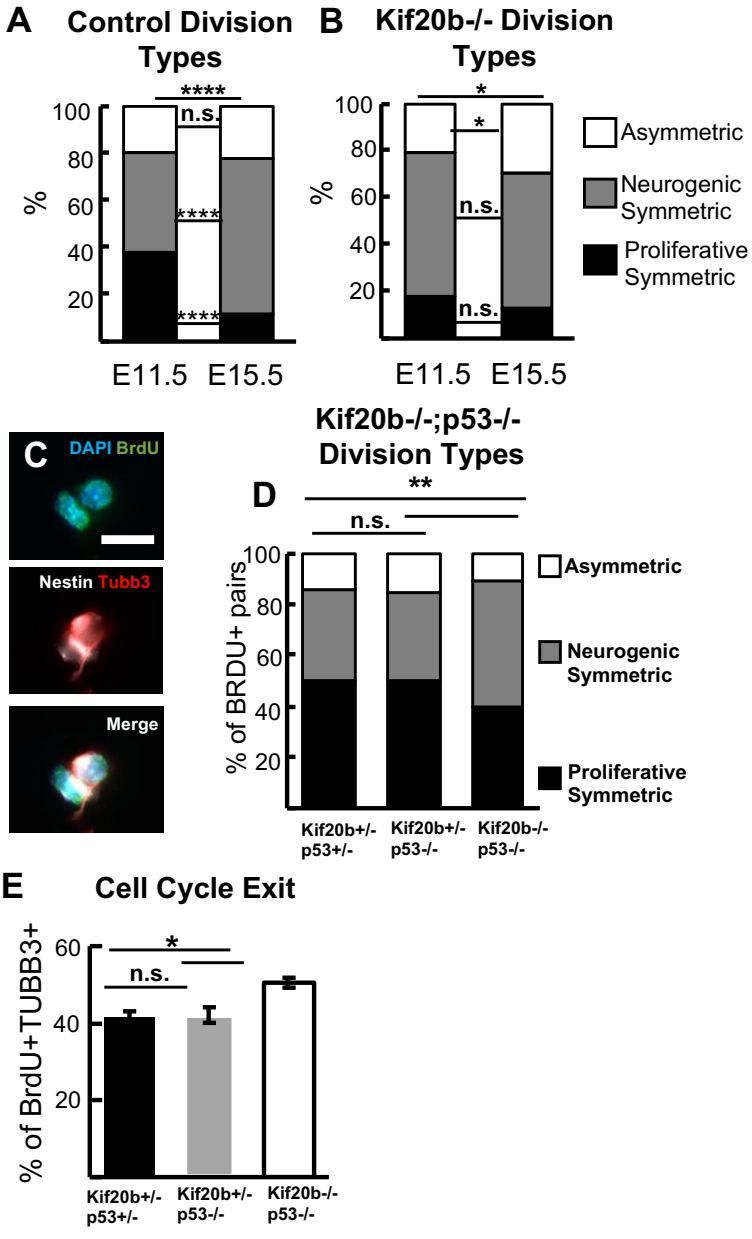

Supplemental Figure 1: The increased neuronal fate of *Kif20b* mutant NESC daughters during early cortical development is not p53-dependent.

(A, B) Comparing division types at different ages (using the same data set as in Figure 5 B, C) shows that control NESCs have significantly more proliferative divisions at E11.5 than E15.5, while *Kif20b* mutants have premature loss of proliferative divisions. For E11.5, n= 394 control (3 +/- and 2 +/+ brains) and 272 *Kif20b-/-* divisions (4 brains). For E15.5, n= 241 control (4 +/- and 1 +/+ brains) and 280 *Kif20b-/-* divisions (5 brains).

(C) Higher density dissociated NESC cultures from E12.5 cortices were treated with Bromodeoxy-Uridine (BrdU) one day before fixation to identify NESC divisions. BrdU+ daughter pairs were classified as one of the three different division types using Nestin (white) and Tubb3 (red).

(D) The increased proportion of neurogenic symmetric divisions was still observed when the *Kif20b* mutant was combined with p53 knockout (*Kif20b-/-; p53-/-),* but was not seen in controls: double heterozygotes (*Kif20b+/-; p53+/-*) or p53 single mutants (*Kif20b+/-; p53-/-*). N=276 control (*Kif20b+/-; p53+/-*) division pairs (3 brains), 228 p53 single mutant (*Kif20b+/-; p53-/-*) division pairs (3 brains), and 270 double mutant (*Kif20b-/-; p53-/-*) division pairs (5 brains).

(E) Cell cycle exit among the daughters of NESC division pairs was scored as daughters that were BrdU+, Tubb3+. The increased cell cycle exit in *Kif20b*-/- daughters is not dependent on p53 function. n= 613 control (*Kif20b+/-; p53+/-*) daughter cells; 689 p53 single mutant daughters (*Kif20b+/-; p53-/-*); and 593 double mutant daughter cells (*Kif20b-/-; p53-/-*).

**** p<0.0001, *** p<0.001, ** p<0.01, * p<0.05, n.s. not significant; chi-square test for populations in A, B, D, E, and Fisher's exact test for individual groups in A and B.

Scale bar, 10μm.